ELSEVIER

Journal of Power Sources 63 (1996) 71–77

JOURNAL OF POWER SOURCES

Low-temperature lithium–manganese oxide cathode materials for polymer batteries

Frédéric Le Cras [b,*], Didier Bloch [a], Pierre Strobel [b]

[a] *Commissariat à l'Energie Atomique/CEREM/DEM, 38054 Grenoble Cedex 9, France*

[b] *Laboratoire de Cristallographie CNRS, BP 166, 38042 Grenoble Cedex 9, France*

Received 1 February 1996; revised 21 May 1996; accepted 2 July 1996

Abstract

Low-temperature spinel phases with physico-chemical characteristics adapted to solid polymer electrolyte environment are prepared as 3 V intercalation material for rechargeable lithium batteries. The lithium intercalation compounds are made by solid-state reaction of an intimate mixture of specifically prepared β-MnO_2 (pyrolusite) and lithium salts at various temperatures between 150 and 450 °C. The experimental results show a direct relation between the composition of the spinel phase obtained and the synthesis temperature. The electrochemical tests show interesting results in terms of reversibility, energy and power density.

Keywords: Manganese oxide spinels; Lithium batteries; Solid polymer electrolytes

1. Introduction

Spinel phases of lithiated manganese dioxides have been thoroughly studied as insertion electrodes materials for rechargeable lithium batteries [1–8]. Three main areas of development exist for the Li/Li–Mn–O system:

1. *4 V systems.* High-voltage $Li_xMn_2O_4$'s ($0 \leq x \leq 1$) show interesting performances for room-temperature rechargeable batteries based on the Li-ion technology (carbon anodes, liquid electrolyte), currently developed for portable equipment [7–9]. Such 4 V systems, however, do not seem suitable for electric vehicle applications, because these may require temperatures in the 50–80 °C range for reasons of local overheating and/or cooling efficiency, whereas the end-member formed by electrochemical extraction of lithium on charge, λ-MnO_2, shows poor thermal stability.
2. *3 V systems: high-temperature spinels.* The intercalation of lithium into $LiMn_2O_4$ (cubic spinel) at ≈ 2.9 V leads to tetragonal $Li_2Mn_2O_4$, due to the Jahn–Teller effect associated with the Mn^{3+} cation [3,7]. This distorsion, together with the rather large volume expansion of the unit cell (6.5%), is supposed to be a major factor in the poor electrochemical reversibility of stoichiometric $LiMn_2O_4$, obtained by the classical, high-temperature process (700–850 °C) [3,7,10]. Other factors that are believed to limit the performance of $LiMn_2O_4$ are low surface area and high crystallinity, which are a consequence of high-temperature treatments.
3. *3 V systems: low-temperature spinels.* Several authors [2,5,11,12] mention the possibility of preparing spinel phases at low temperatures (350–450 °C) for the stoichiometric ratio Li:Mn = 0.5. The improvement in electrochemical results (capacities around 100–130 mAh/g [3]) is partly ascribed to (i) a high specific surface area and (ii) a lower crystallinity of the low-temperature spinel.

Of particular interest are the spinel phases with a manganese oxidation state close to +4 [3,13], situated in the triangle $LiMn_2O_4$–$Li_2Mn_4O_9$–$Li_4Mn_5O_{12}$ of the Li–Mn–O composition-valence diagram [14,15] (see gray area in Fig. 1). These spinel structures are also characterized by a Li:Mn ratio x in the 0.5–0.8 range. Although a fraction of the capacity is revealed at 4 V (to some extent, for the portion of the intercalation line above the $LiMn_2O_4$–$Li_4Mn_5O_{12}$ 'stoichiometric line' in Fig. 1), capacities between 120–180 mAh/g are achieved at 3 V [16] apparently for three main reasons: (i) the theoretical energy densities are the highest among all 3 V spinel phases [3,17]; (ii) the cubic symmetry is supposed to be maintained during the largest part of lithium insertion, and (iii) the smaller amount of Mn^{3+} in spinels with high Li:Mn ratio x minimizes the possible disproportionation reaction: $2Mn^{3+} \rightarrow Mn^{4+} + Mn^{2+}$ which is supposed to cause the dissolution of manganese in the electrolyte and affect the cycling efficiency [18].

* Corresponding author.

PII S0378-7753(96)02448-2

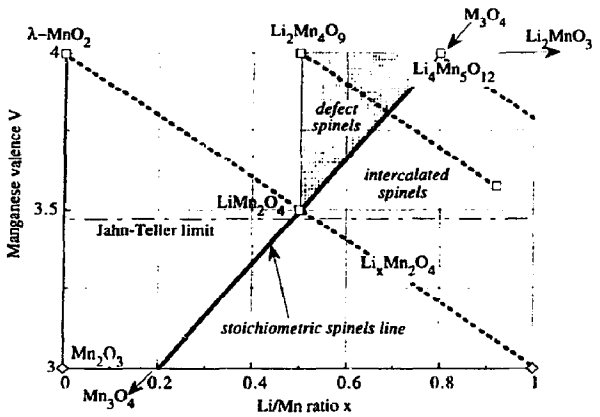

Fig. 1. Composition–valence diagram of Li-Mn-O spinels: (———) stoichiometric spinels (stoichiometry M_3O_4), and (– – –) lithium intercalation lines. The region of interest (triangle $LiMn_2O_4$-$Li_2Mn_4O_9$-$Li_4Mn_5O_{12}$) is shaded.

'Low-temperature' Li–Mn–O spinels have been prepared either with electrolytic γ-MnO_2 or $MnCO_3$ at 400–600 °C [3,5], or by sol–gel techniques [19]. In these works, high experimental energy densities and capacity retentions were correlated to high specific surface area ($>50\ m^2/g$) and low crystallinity of the active material. Using high specific surface area precursor materials presents several advantages: (i) increased reactivity at low temperatures; (ii) good adaptation to liquid electrolyte technologies: the liquid electrolyte penetrates the pores of the grain of active material and enhances the electrode surface, thus improving the exchanges during the electrochemical reaction, and (iii) experimental evidence of improved electrochemical performances.

This explains why most of the previous studies neglected the preparation of Li–Mn–O spinels from precursors with low specific surface area. Moreover, low specific surface area is often correlated with high crystallinity, which is not a desired target.

In the case of solid polymer electrolyte (SPE), however, the use of a high porosity and high specific surface area material must be avoided, because the electrolyte is not able to penetrate its pores. Non-porous, low specific area particles are needed in this case to obtain high energy densities and to prevent the damaging presence (in terms of energy density) of voids in the thin film cathode.

To our knowledge, there is no report of complete solid state reaction below 400 °C, neither of any relation between the synthesis temperature and the composition of the final spinel phase. Our previous study [14], using commercial manganese oxide precursors (carbonate, β- and γ-MnO_2) confirmed the difficulty of achieving complete reactions in this temperature range. In the case of β-MnO_2, a quantitative analysis of X-ray patterns showed that the amount of residual dioxide was correlated with the processing temperature and was at least 8% at 450 °C (see Fig. 6 in Ref. [14]).

β-MnO_2 is indeed considered as the least reactive form of manganese dioxide due to its strictly stoichiometry and usually large grain size, and we are not aware of other works using it as a manganese starting reagent in Li–Mn–O syntheses. On the other hand, the exact stoichiometry can be an asset (the starting Mn oxidation state is exactly +4).

We will show in this paper that the apparent drawbacks of β-MnO_2 (supposed poor reactivity and morphological limitations) can be overcome by a specific preparation, and that this starting reagent gives excellent reactivity at low temperatures. This work describes the synthesis and electrochemical properties of Li–Mn–O spinel compounds obtained by complete solid-state reactions at temperatures ≤ 500 °C. In addition, a correlation between the reaction temperature and the actual composition of the equilibrium $Li_{1+\alpha}Mn_{2-\alpha}O_4$ stoichiometric spinel phase in this system will be established. Note that by 'stoichiometric spinel', we mean here any compound having a cation/ratio equal to 3:4, i.e. lying along the $LiMn_2O_4$–$Li_4Mn_5O_{12}$ line in Fig. 1.

2. Experimental

2.1. Preparation

Lithium–manganese spinel phases are prepared by solid state reactions of lithium salts and β-MnO_2 with initial Li:Mn ratios in the 0.5–0.8 range. Powders of specifically prepared β-MnO_2 (Sedema) and Li_2CO_3 (Merck) or hydrated LiOH (Prolabo) are thoroughly mixed by ball-milling, and heat-treated under oxygen flow in a rotating furnace equipped with a continuous milling device [20]. Samples are collected periodically during thermal treatment in order to follow the advancement of the reaction.

2.2. Characterization

Powder X-ray diffraction is carried out on a automated Siemens D-5000 diffractometer with Cu $K\alpha_1$ radiation. The lattice constants are refined by a least-squares method (full pattern matching).

The manganese content and the manganese oxidation state are determined by oxido-reduction titrations. The lithium content of the final spinel phase is given either as the Li:Mn initial ratio (when the final product is constituted by a single spinel phase), or calculated with the justified assumption that the final mixture is constituted by a stoichiometric spinel phase and another single known residual phase [14].

2.3. Electrochemical testing

The cathodic composite electrode slurry containing lithium–manganese oxide is prepared by mixing e.g. the active material (50% vol.), carbon black (SN2A, Berre, France; 10% vol.), PEO (Aldrich, molar mass 600 000, 40% vol.) and Li–TFSI (3 M) in distilled water. The EO:Li ratio is ~ 14:1. The slurry is spread onto a nickel current collector (10 μm thick, Goodfellow). The PEO/Li–TFSI electrolyte is prepared the same way, and cast onto the cathodic layer

[21]. After evaporation of the solvent, the total thickness of the nickel-cathode-electrolyte sandwich is lower than 100 μm. This sandwich is dried under vacuum at 115 °C during 48 h. Li/polymer electrolyte/Li_xMnO_2 cells with an active area of 50 cm^2 are assembled in a glove box, using a lithium foil anode (MetallGes., 200 μm). The capacity of these cells is in the range 0.5–2 mAh cm^{-2}. They are placed in an oven and tested between 77 and 110 °C. The electrochemical tests are carried out using a 'Mac-Pile' (Bio-logic, Claix, France) in a potentiostatic or galvanostatic mode. The voltage is scanned at various rates between 10 and 120 mV/h. Discharge current densities are in the 0.25–0.50 range mA/cm^2.

3. Results and discussion

3.1. Stoichiometry vs. treatment temperature

All the final products are characterized by a low specific surface area (~ 2 m^2/g), a high density (close to the theoretical density 4.2) and high crystallinity. The X-ray analysis shows that the reaction between β-MnO_2 and the lithium salt can go to completion within reasonable periods of time, even at very low temperatures: As an example, Fig. 2 shows the evolution of the X-ray pattern with heating time for a sample treated at 200 °C (sample 85). Here the β-MnO_2 phase has completely disappeared after 75 h, and a well-defined spinel structure with sharp diffraction lines is formed. The same result is achieved after 10 h at 250 °C, see Fig. 3.

In both these samples, an intermediate phase is formed during the earlier stages of the β-MnO_2 → spinel transformation and disappears with time. The characterization of this phase, which may constitute a 'buffer' structure between the β-MnO_2 rutile structure and the final cubic spinel structure, is in progress [22].

X-ray diffraction also showed the presence in most synthesis runs of a lithium-containing residual phase ($LiOH \cdot H_2O$ or Li_2CO_3 below 300 °C, Li_2MnO_3 at 350 °C and higher temperatures) after complete transformation of the β-MnO_2 reagent. Assuming that the spinel phase formed

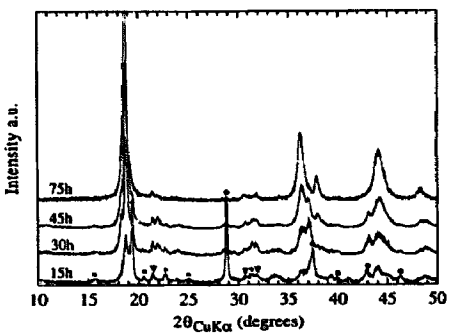

Fig. 2. Powder X-ray diffraction patterns of sample 85 (initial Li:Mn ratio: 0.8) at different stages of the thermal treatment at 200 °C. The Li:Mn ratio of the final stoichiometric spinel structure is around 0.56. Other remaining phases: (●) β-MnO_2; (▼) Li_2CO_3; (♦) $LiOH \cdot H_2O$, and (■) intermediate phase (see text).

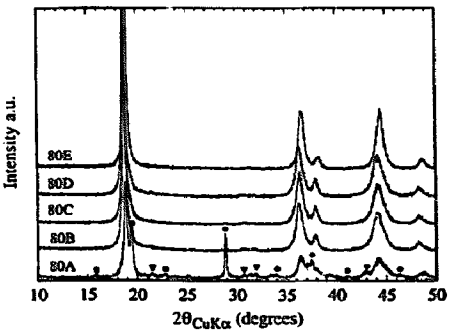

Fig. 3. Powder X-ray diffraction patterns of sample 80 (initial Li:Mn: 0.65) at different stages of the thermal treatment. From bottom to top: (A) 5 h; (B) 10 h; (C) 15 h; (D) 20 h at $T = 250$ °C, (E) +5 h at 400 °C. Impurity symbols as in Fig. 2.

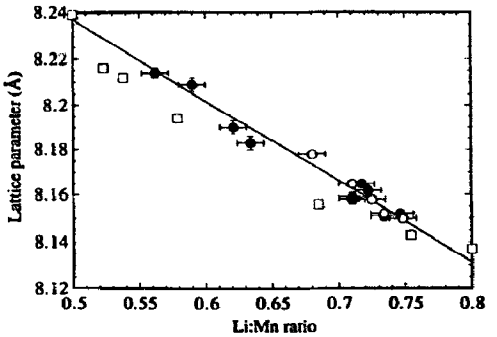

Fig. 4. Lattice constants of Li–Mn–O spinel phases as a function of Li:Mn: (○) data above 500 °C apply to systems with initial Li:Mn ratio equal to 0.8y, and (□) data refer to literature values.

is stoichiometrically, i.e. obeys formulas such as $Li_{1+\alpha}Mn_{2-\alpha}O_4$ or $Li_xMnO_{4(1+x)/3}$ (the former emphasizing the constant cation/anion ratio, and the latter the Li/Mn ratio x), the two-phase system is completely determined by the measurement of the average manganese valence of the two-phase mixture V_0 and the initial Li:Mn ratio x_0 [14]. The key assumption here is the stoichiometric nature of the spinel phase, which imposes a correlation between the Li:Mn ratio x and the manganese valence in the stoichiometric spinel phase $V = (8 + 5x)/3$, deduced from the equivalent formulas

$$Li_xMnO_{4(1+x)/3} = Li_xMnO_{(x+V)/2} \quad (1)$$

This assumption is confirmed by the good agreement between: (i) experimental lattice parameters and literature values (see Fig. 4), and (ii) experimental and calculated manganese contents.

The analytical relationships giving x and V as a function of x_0 and V_0 have been described elsewhere [14]. Table 1 gives the x and V values (as well as cell parameter values) for various spinel phases obtained as a function of synthesis temperature, T. The variation of x with T (see Fig. 5) shows a clear correlation between the composition of the spinel phase formed and the processing temperature. Up to about 500 °C, a given value of x ($0.5 \leq x \leq 0.75$) corresponds to a given value of the temperature T_x ($200\,°C \leq T_x \leq 500\,°C$) and v.v.

Table 1
Characterization of final spinel phases formed as a function of reaction temperature

Synthesis temperature (°C)	Sample	Li:Mn ratio, x (±0.01)	Lattice constant a (Å)	Mn valence, V (±0.015)
200	85D	0.562	8.214(2)	3.60
250	80D	0.59	8.209(3)	3.645
250	83E	0.566		3.61
300	85E	0.621	8.190(3)	3.70
350	75C	0.634	8.183(3)	3.724
400	75E	0.717	8.165(1)	3.86
400	85F	0.722	8.162(3)	3.87
400	79K	0.71	8.159(2)	3.85
400	83G	0.71	8.158(2)	3.85
420	85G	0.734	8.151(1)	3.89
450	75F	0.746	8.152(1)	3.91
500	75G	0.748	8.150(1)	3.914
550	75H	0.734	8.152(1)	3.89
550	5H	0.725		3.875
600	75I	0.725	8.158(1)	3.876

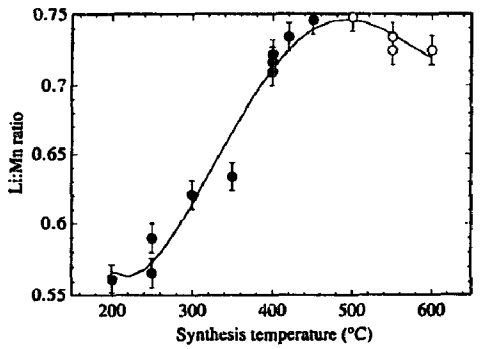

Fig. 5. Composition of the stoichiometric spinel phases synthesized by reacting β-MnO_2 with LiOH or Li_2CO_3 as a function of treatment temperature. (○) and (□) as in Fig. 4.

What happens if $T \neq T_x$? Several cases may occur.

(i) $T < T_x$. Within a few hours, β-MnO_2 reacts completely to form a stoichiometric spinel with $x < x_0$. The mixture contains residual lithium reagent, and the proportions of the two phases do not change anymore even if longer reaction times are used. As an example, the evolution of sample 80 (initial Li:Mn value $x_0 = 0.65$) for variable heat-treatment durations is given in Table 2 and Fig. 3. After 10 h at 250 °C (sample 80B), β-MnO_2 is not detectable any longer. A stoichiometry calculation shows that around 6 mol% of the initial LiOH remains (mostly as carbonate). The formula of the spinel phase is now $Li_{0.59}Mn^{3.65+}O_{2.12}$. Extending the thermal treatment at 250 °C to 15 h, then to 20 h brings no change in the average manganese oxidation state. The fact that the two-phase system is 'fixed' is confirmed by the lattice parameter of the spinel formed, which is also constant at ~8.209 Å, see Table 2.

(ii) $T_x < 500$ °C. Two cases must be distinguished here. If the initial mixture is quickly heated to temperature T, the stoichiometric spinel formed has $x > x_0$, the lithium precursor is entirely consumed and some β-MnO_2 remains in the final mixture. For low heating rates, on the other hand, the reaction mixture has time to equilibrate at intermediate temperatures ($T < T_x$), giving $x < x_0$ and excess lithium precursor in the first stages of the reaction, as in case 1. As the temperature rises, the residual lithium salt reacts progressively, x and V in the spinel phase increase until the equilibrium composition at temperature T_x is reached, see Fig. 5. This evolution corresponds to the reaction

$$Li_xMnO^4_{3(1+x)} + \frac{5\epsilon}{12}O_2 + \frac{\epsilon}{2}Li_2CO_3 \rightarrow Li_{x+\epsilon}MnO^4_{3(1+x+\epsilon)} + \frac{\epsilon}{2}CO_2 \quad (2)$$

Note that reaction (2) illustrates a tendency for the manganese ion to oxidize below ~500 °C. In fact, it corresponds to a composition point moving up and right along the $LiMn_2O_4$–$Li_4Mn_5O_{12}$ line in Fig. 1.

Reaction (2) is probably constituted by a two-stage process, as the stoichiometric spinel structure transforms first partly into Li_2MnO_3 (at $T > 300$ °C) prior to producing a stoichiometric spinel phase of higher manganese oxidation state, according to the reaction

$$Li_xMnO^4_{3(1+x)} + \frac{5\epsilon}{12}O_2 + \frac{\epsilon}{2}Li_2CO_3 \xrightarrow{300-350\ °C} \frac{1-\epsilon}{2-x}Li_xMnO^4_{3(1+x)} + \frac{\epsilon(8x+11)}{6(2-x)}O_2 + \frac{\epsilon}{2-x}Li_2MnO_3 + \frac{\epsilon}{2}CO_2 \xrightarrow{T'>T} Li_{x+\epsilon}MnO^4_{3(1+x+\epsilon)} + \frac{\epsilon}{2}CO_2 \quad (3)$$

When $T = T_x$, the composition of the spinel phase is $Li_xMnO_{4(1+x)/3}$ and corresponds to a complete reaction between both precursors. Above T_x, it may be possible to synthesize a defect spinel, with same Li:Mn ratio x but with higher manganese oxidation state (i.e. moving up vertically from the stoichiometric spinel line in Fig. 1). This happened for sample 80E treated at 400 °C after a first equilibration at 250 °C, see Table 2. From Fig. 5, T_x for this sample ($x_0 = 0.65$) is ≈370 °C. During the temperature increase from 250 to 370 °C, the remaining lithium carbonate reacts progressively. At 370 °C, the composition of the stoichiometric spinel formed corresponds to the initial Li:Mn ratio, i.e. $Li_{0.65}Mn^{3.75+}O_{2.2}$. A subsequent 5 h annealing at 400 °C raises the manganese oxidation state of the final product to 3.83, whereas it remains single-phase and its lattice constant decreases to 8.158 Å: its composition is now $Li_{1.161}Mn_{1.786}O_4$, i.e. the cation/anion has decreased to 0.737. The stoichiometric spinel has incorporated oxygen and transformed into a defect spinel structure containing 0.053 vacant cationic sites per spinel formula unit.

Table 2
Evolution of the products of the reaction β-MnO_2 + LiOH with reaction time at 250 and 400 °C (initial Li:Mn ratio 0.65)

Sample	T (°C)	Duration (h)	V_0 [a]	V [b]	Spinel lattice constant (Å)	Secondary phases, remarks
80A	250	5	3.70	[c]	8.208(2)	β-MnO_2, Li_2CO_3, intermediate phase
80B	250	10	3.635	[c]	8.209(3)	Li_2CO_3, traces of intermediate phase
80C	250	15	3.647	3.647	8.211(3)	Li_2CO_3
80D	250	20	3.645	3.645	8.209(3)	Li_2CO_3
80E	400	5	3.826	3.826	8.158(2)	defect spinel

[a] Average overall Mn valence (±0.015).
[b] Actual Mn valence in the resulting spinel phase (±0.015).
[c] Not determined (more than 1 foreign phase).

Fig. 5 shows that there is a maximum manganese oxidation state and Li:Mn ratio attainable in our operating conditions: above ~500 °C, the stable Mn^{4+} compound Li_2MnO_3 grows at the expense of the spinel phase, inducing a decrease in x and V according to the reaction

$$Li_xMnO_{\frac{4}{3}(1+x)} \rightarrow \frac{\epsilon}{2}Li_2MnO_3 + Li_{x-\epsilon}Mn_{1-\frac{\epsilon}{2}}O_{\frac{4}{3}(x+1-3\frac{\epsilon}{2})} + \frac{\epsilon}{4}O_2 \quad (4)$$

with $0.5 < (x-\epsilon)/(1-\epsilon/2) < 0.8$.

This explains the maximum Li:Mn = 0.75 ratio observed for the spinel structure formed at about 500 °C, even when the Li:Mn initial ratio is equal to 0.8. The formula of the spinel phase becomes here $Li_{2.25}Mn_3O_7$. Unfortunately, this mechanism seems to prevent, in these operating conditions, the formation of spinel phases with manganese oxidation state V higher than 3.92 and of Li:Mn ratios higher than 0.75.

Fig. 5 also shows that even at very low temperatures ($\leq$ 300 °C), the high initial manganese oxidation state of the β-MnO_2 precursor cannot be maintained. At 150 °C, β-MnO_2 is completely reacted after ≈ 150 h of thermal treatment, giving mostly the intermediate phase mentioned above. No reaction is observed under ≈ 150 °C.

Nevertheless, our results demonstrate the possibility to synthesize spinel compounds of the desired manganese valence $3.5 \leq V \leq \approx 3.92$ by an all-solid state process between 200 and 500 °C, within reasonable periods of time [20].

3.2. Electrochemical cycling behaviour

The cycling capacity of a Li_xMnO_y/PEO–Li–TFSI/Li cell containing sample 63 (Li:Mn = 0.66) is shown in Fig. 6. The cycling conditions are the following: voltage window 3.1 (end of charge) to 2.7 V (end of discharge), mean discharge voltage ≈ 2.85 V, discharge rate $C/5$, temperature 110 °C. In these conditions, the capacity of sample 63 remains around 100 mAh/g at the end of the 35th cycle. The stability of this system is further illustrated in Fig. 7, which shows galvanostatic charge/discharge characteristics for cycles 20 to 60. These performances were confirmed in liquid electrolyte cells, with capacities in the 140 mAh/g range at the 20th cycle for sample 63 (cycled between 2.0 and 3.5 V) [17].

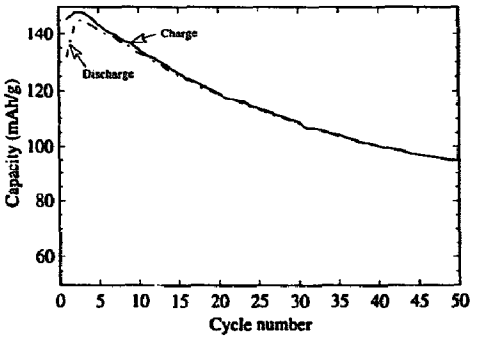

Fig. 6. Energy density as a function of cycle number for sample 63 (Li:Mn = 0.66) tested in a solid electrolyte cell at 110 °C and $C/5$ rate (voltage limits 3.1–2.7 V).

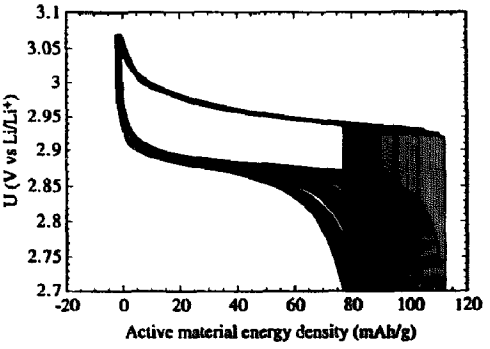

Fig. 7. Galvanostatic cycling characteristics of cell 178 ($I_c \approx C/10$ and $I_d \approx C/3$, cycles 20 to 60, 110 °C).

3.3. Kinetic study

Fig. 8 shows the results of cyclic voltammetry of a Li/PEO–Li–TFSI/spinel cell, studied at various scan rates between 25 and 150 mV/h at 110 °C. The sample used (# 79 K) has a Li:Mn ratio equal to 0.71. Even at high rates of discharge ($C/2$), the polarization of the electrode remains very small, indicating a good reversibility behaviour. Note that we use a normalized intensity scale (in mA/g of active material), to allow an easy evaluation of the discharge rate: for a theoretical 3 V capacity of ≈ 150 mAh/g, an average

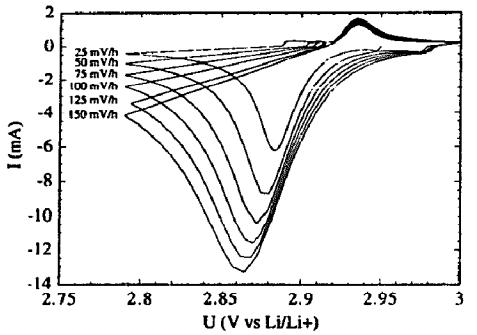

Fig. 8. Cyclic voltammograms of sample 79 (Li:Mn = 0.71, solid electrolyte cell, 110 °C, 123 mg of active material) at various sweep rates (left constant at 5 mV/h during the charge).

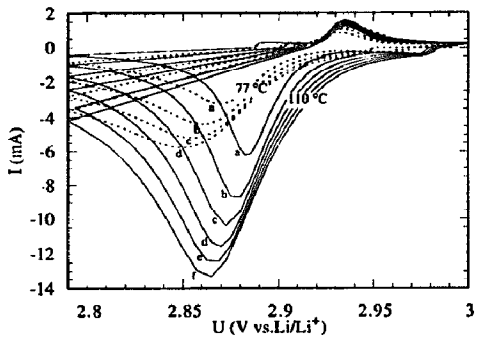

Fig. 9. Comparison of cyclic voltammograms of sample 79 (Li:Mn = 0.71) at two different temperatures (sweep rates during the discharge (a) 25, (b) 50, (c) 75, (d) 100, (e) 125, (f) 150 mV/h, left constant at 5 mV/h during the charge).

normalized current of 75 mA/g, for example, corresponds to a $C/2$ regime.

A comparative kinetic study of sample 79 at 110 and 77 °C (see Fig. 9) shows an increased polarization at 77 °C. It remains sufficient low to sustain the $C/3$ or $C/4$ rates of discharge at this temperature. This constitutes a good target for traction batteries. These results also show the absence of strong influence of the low specific surface area of the active material on the kinetics of the electrochemical reaction, even at higher rates of discharge (tests up to a C regime).

4. Conclusions

The possibility of preparing manganese oxide-based cathode active materials with specific physico-chemical characteristics adapted to solid polymer electrolyte for rechargeable lithium batteries has been investigated. Complete solid state reaction, within reasonable periods of time, between suitably prepared β-MnO_2 and lithium hydroxide or carbonate has been achieved, even at temperatures ≤ 200 °C. The final product of the reaction is a stoichiometric or a defect spinel phase with a composition and manganese valence determined by the synthesis conditions (temperature and heating rate). Note that the composition–temperature relationship found here (see Fig. 5) corresponds to a subtle interplay between stoichiometric spinel composition and fractions of excess Mn or Li reagents. A quite different phenomenon occurs at high temperatures (>900 °C), where recent thermogravimetric studies have shown a reversible oxygen loss from single-phase $LiMn_2O_4$ spinel [23].

Spinel phases obtained in these conditions are characterized by: high chemical purity, low specific surface area, low particle size, low porosity, high density and high crystalline quality.

Depending on the Li:Mn initial ratio and the temperature synthesis, high manganese valence spinel phases (up to +3.92), with lattice constants in the 8.13–8.16 Å range, have been manufactured. Used as active material in lithium insertion electrodes, these products show interesting electrochemical reversibility and kinetics behaviour. Due to their performances, which seem not to be strongly affected by the low specific surface area or high crystallinity, they may be suitable for solid polymer electrolyte as well as for liquid electrolyte lithium batteries.

Acknowledgements

This study has been carried out in the framework of a European Community 'Joule II' Programme (contract CT92-0146), associating the authors (CEA and CNRS, Grenoble) with: Sedema, Tertre, Belgium (J.C. Rousche, J.B. Soupart); Bolloré Technologies, Quimper, France (H. Majastre), and EDF, Centre de Recherches des Renardières, Moret-sur-Loing, France (P. Baudry).

The authors also thank all co-workers in Grenoble for their collaboration, especially J.M. Bouvier, P. Clement, N. Lebrun, G. Lonchampt, R. Louis, C. Nicotra and M. Richaud (CEA), and M. Anne (CNRS).

References

[1] W.J. Macklin, R.J. Neat and R.J. Powell, *J. Power Sources, 34* (1991) 39.
[2] F.K. Shokooki, J.M. Tarascon, B.J. Wilkens, D. Guyomard and C.C. Chang, *J. Electrochem. Soc., 139* (1992) 1845.
[3] M.M. Thackeray, A. de Kock, M.H. Rossouw, D. Liles, R. Bitthin and D. Hoge, *J. Electrochem. Soc., 139* (1992) 363.
[4] A. de Kock, M.H. Rossouw, L.A. de Piccioto, M.M. Thackeray, W.I.F. David and R.M. Ibberson, *Mater. Res. Bull., 25* (1990) 657.
[5] G. Pistoia, G. Wang and C. Wang, *Solid State Ionics, 58* (1992) 285.
[6] M. Armand, J.M. Chabagno and M.J. Duclot, in P. Vashita (ed.), *Fast Ion Transport in Solids*, North-Holland, Amsterdam, 1979, p. 131.
[7] J.M. Tarascon and D. Guyomard, *J. Electrochem. Soc., 138* (1991) 2864.
[8] J.M. Tarascon, E. Wang and F.K. Shokoohi, *J. Electrochem. Soc., 138* (1991).2859.
[9] D. Guyomard and J.M. Tarascon, *J. Electrochem. Soc., 139* (1992) 937.
[10] S. Yamada, T. Ohsaki, K. Inada, N. Chiba H. Nose and T. Uchida, in S. Subbarao, V.R. Koch, B.B. Owens and W.H. Smyrl (eds.), *Symp. Rechargeable Batteries, Meet. The Electrochemical Society, Hollywood, FL, USA, 1989*, Proc. Vol. 90-5, 1990, p. 21.

[11] J.N. Reimers, E.W. Fuller, E. Rossen and J.R. Dahn, *J. Electrochem. Soc.*, *140* (1993) 3396.
[12] W.F. Howard, Jr., *Ext. Abstr., 7th Int. Meet. Lithium Batteries, Boston, MA, USA, 15–20 May 1994*, p. 285.
[13] M.M. Thackeray and A. de Kock and W.I.F. David, *Mater. Res. Bull.*, *28* (1993) 1041.
[14] F. Le Cras, P. Strobel, M. Anne, D. Bloch, J.B. Soupart and J.C. Rousche, *Eur. J. Solid State Chem.*, *33* (1996) 67.
[15] P. Strobel, F. Le Cras and M. Anne, *J. Solid State Chem.*, *124* (1996) 83.
[16] M.M. Thackeray, *Prog. Batteries Battery Mater.*, *11* (1992) 150.
[17] F. Le Cras, D. Bloch, M. Anne and P. Strobel, *Mater. Res. Soc. Symp. Proc.*, *369* (1995) 39.
[18] R.J. Gummov, A. de Kock and M.M. Thackeray, *Solid State Ionics*, *69* (1994) 59.
[19] S. Bach, M. Henry, N. Baffier and J. Livage, *J. Solid State Chem.*, *88* (1990) 325.
[20] D. Bloch, F. Le Cras and P. Strobel, *Fr. Patent No. 94 07 569* (1994).
[21] G. Lonchampt, *Fr. Patent No. 92 06 129* (1992).
[22] F. Le Cras, *Ph.D. Thesis*, University J. Fourier, Grenoble (1996); F. Le Cras, P. Strobel, M. Anne and D. Bloch, to be published.
[23] J.M. Tarascon, W.R. McKinnon, F. Coowar, T.N. Bowmer, G. Amatucci and D. Guyomard, *J. Electrochem. Soc.*, 141 (1994) 1421.